Cosserat Rod-based Kinetostatic Analysis of a 6-$\overline{R}$US Parallel Continuum Robot

Vinay Rodrigues, Bingbin Yu, Christoph Stoeffler, and Shivesh Kumar

19th International Symposium on
ADVANCES IN ROBOT KINEMATICS
LJUBLJANA, JUNE 30 – JULY 4, 2024

DFKI Robotics Innovation Center Bremen

Introduction

Parallel Continuum Robot (PCR)

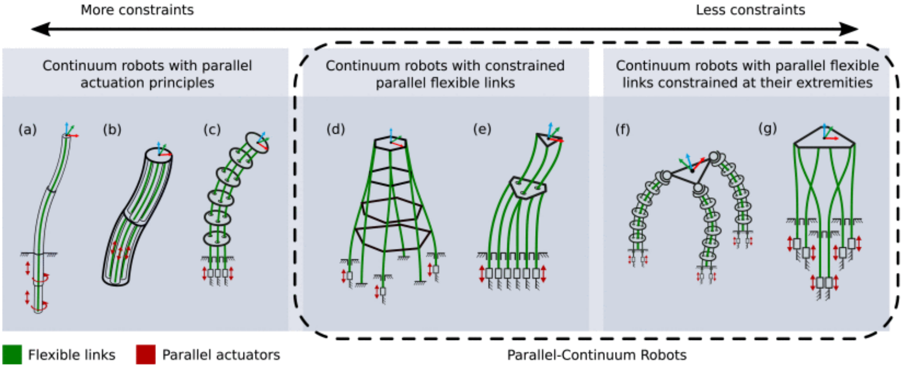

Figure: Spectrum of continuum manipulators. [1]

Motivation

Robot structure

- Six compliant legs
- 6-$\underline{R}$US kinematic structure
- Active actuation at each leg
- Titanium alloy material

Contribution

- Boundary conditions for 6-$\underline{R}$US PCR
- Position and stiffness analysis
- Workspace evaluation for the PCR

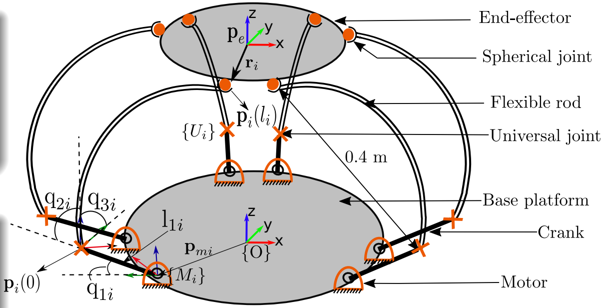

Figure: 6-$\overline{R}$US Parallel Continuum Robot (PCR)

Literature

(a) Geometry-based approach

- Configurations are characterized by specific geometric functions.
- Simplify the modelling process and computationally efficient.
- Inverse kinematic problem can be solved analytically.

(b) Mechanics-based approach

- Robots are defined as a function of material properties
- Classical elasticity theories, Lumped parameter model, FEA.

(c) Data-based approach

- Computationally expensive for mechanics motivated problems
- Offline and online algorithms

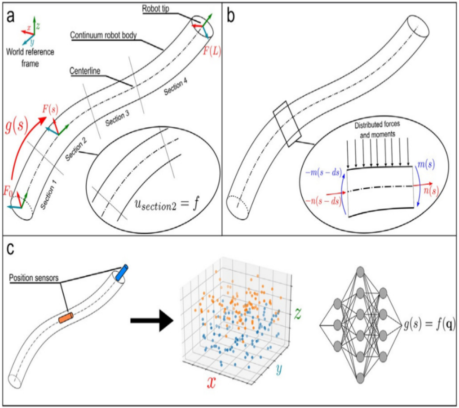

Figure: Classification of modelling approaches for continuum robots into three primary categories: (a)Geometry-based (b) Mechanics-based and (c) Data-based modelling techniques [3]

Theory

Kinematics and mechanics

- $\mathbf{p}(s_i) \in \mathbb{R}^3$ and $\mathbf{R}(s_i) \in SO(3)$
- $s_i \in [0, L]$ is length of the flexible link.
- $\mathbf{g}(s_i) \in SE(3)$:

$$\mathbf{g}(s_i) = \begin{bmatrix} \mathbf{R}(s_i) & \mathbf{p}(s_i) \\ 0 & 1 \end{bmatrix}$$

- $\mathbf{v}(s) \in \mathbb{R}^3$ and $\mathbf{u}(s) \in \mathbb{R}^3$ represent the linear and angular rates of change of $\mathbf{g}(s)$ in link's local frame.
- $\mathbf{f}(s_i) \in \mathbb{R}^3$ and $\mathbf{l}(s_i) \in \mathbb{R}^3$ are the force and moment, respectively, applied per unit length i.
- $\mathbf{n}(s_i) \in \mathbb{R}^3$ and $\mathbf{m}(s_i) \in \mathbb{R}^3$ are the internal force and moment in global coordinate frame.

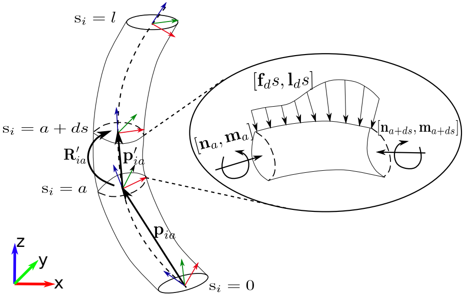

Figure: Deformation of a continuum section *ds* under load

Elasticity model

- Linear material constitutive model
- $\mathbf{K}_{se} \in \mathbb{R}^{3\times 3}$ and $\mathbf{K}_{bt} \in \mathbb{R}^{3\times 3}$ depict the mechanical stiffness matrices for unit length.
- A : area of cross-section
- G: Modulus of Rigidity
- E: Young's Modulus,
- I_{xx} and I_{yy} are the second moment of inertia about the x & y axes.

$$\mathbf{n}_i(s) = \mathbf{R}_i(s)\mathbf{K}_{SE,i}(\mathbf{v}_i(s) - \mathbf{v}_i^*(s))$$
$$\mathbf{m}_i(s) = \mathbf{R}_i(s)\mathbf{K}_{BT,i}(\mathbf{u}_i(s) - \mathbf{u}_i^*(s))$$

where

$$\mathbf{K}_{SE,i}(s) = \begin{bmatrix} G_iA_i(s) & 0 & 0 \\ 0 & G_iA_i(s) & 0 \\ 0 & 0 & E_iA_i(s) \end{bmatrix}$$

,

$$\mathbf{K}_{BT,i}(s) = \begin{bmatrix} EI_{xx,i}(s) & 0 & 0 \\ 0 & EI_{yy,i}(s) & 0 \\ 0 & 0 & G(I_{xx,i} + I_{yy,i}) \end{bmatrix}$$

$$\mathbf{p}_i' = \mathbf{R}_i \mathbf{v}_i;$$

$$\mathbf{R}_i' = \mathbf{R}_i \hat{\mathbf{u}}_i;$$

$$\mathbf{n}_i' = -\mathbf{f}_i$$

$$\mathbf{m}_i' = -\mathbf{p}_i' \times \mathbf{n}_i - \mathbf{l}_i$$

$$\mathbf{v}_i = \mathbf{K}_{SE,i}^{-1} \mathbf{R}_i^T \mathbf{n}_i + \mathbf{v}_i^*$$

$$\mathbf{u}_i = \mathbf{K}_{BT,i}^{-1} \mathbf{R}_i^T \mathbf{m}_i + \mathbf{u}_i^*$$

Figure: For each flexible link i, a system of differential equations describes the evolution of the state variables $\mathbf{p}_i$, $\mathbf{R}_i$, $\mathbf{n}_i$, and $\mathbf{m}_i$ with respect to s_i.

Modelling

Boundary conditions

Force bal. (3 eqs): $\sum_{i=0}^{n}[\mathbf{n}_i(l_i)] - \mathbf{F} <= 5e^{-10}$

Moment bal. (3 eqs): $\sum_{i=0}^{n}[\mathbf{p}_i(l_i) \times \mathbf{n}_i(l_i) + \mathbf{m}_i(l_i)] - \mathbf{p}_e \times \mathbf{F} - \mathbf{M} <= 5e^{-10}$

Dist. const.(3x6 eqs): $\mathbf{p}_e + \mathbf{R}_e\mathbf{r}_i - \mathbf{p}_i(l_i) <= 5e^{-10}$

Moment const.(3x6 eqs: $\mathbf{m}_i(l_i) <= 5e^{-10}$

Joint angle const.: $-20^\circ \leq q_{1i} \leq 90^\circ \qquad (i = 1, ..., 6)$

Figure: Limits imposed on the constraints (units: meters & newton-meters).

High level Working of the Solver

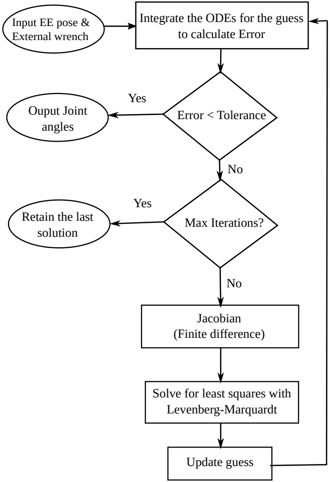

Figure: Shooting method implementation to solve for the BVPs [2]

Inverse and forward formulation

$$\left.\begin{array}{ll} \mathbf{p}_e & \in \mathbb{R}^3 \\ \mathbf{R}_e & \in SO(3) \\ \mathbf{F} & \in \mathbb{R}^3 \\ \mathbf{M} & \in \mathbb{R}^3 \\ \mathbf{B}_{IK} & \in \mathbb{R}^{42} \\ \mathbf{H}_0 & \in SE(3) \end{array}\right. \longrightarrow \boxed{\text{Inverse model}} \longrightarrow \begin{array}{c} \mathbf{q}_{1i} \in \mathbb{R}^6 \\ (i = 1, ..., 6) \end{array}$$

where $\mathbf{B}_{IK} = [n_{x,1}(0), n_{y,1}(0), n_{z,1}(0), m_{z,1}(0), q_{11}, q_{21}, q_{31}, \ldots]^T$

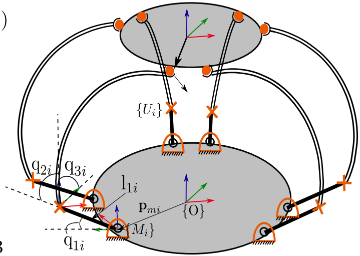

$$\left.\begin{array}{ll} \mathbf{q}_{1i} & \in \mathbb{R}^6 \\ \mathbf{F} & \in \mathbb{R}^3 \\ \mathbf{M} & \in \mathbb{R}^3 \\ \mathbf{B}_{FK} & \in \mathbb{R}^{42} \\ \mathbf{H}_0 & \in SE(3) \end{array}\right. \longrightarrow \boxed{\text{Forward model}} \longrightarrow \begin{array}{l} \mathbf{p}_e \in \mathbb{R}^3 \\ \mathbf{R}_e \in SO(3) \end{array}$$

where $\mathbf{B}_{FK} = [n_{x,1}(0), n_{y,1}(0), n_{z,1}(0), m_{z,1}(0), q_{21}, q_{31}, \ldots, \mathbf{p}_e, \mathbf{R}_e]^T$

Results

Circular trajectory with R 0.25m

Helical trajectory with R 0.25m, H 0.15m

Trajectory Comparison under Constant Load

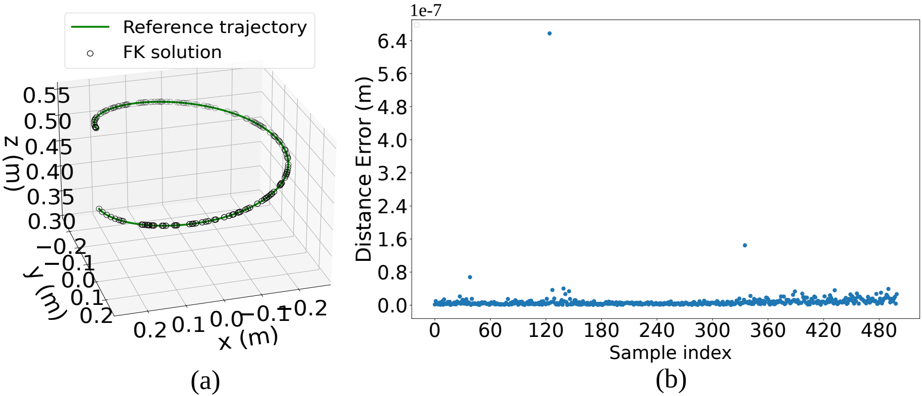

Figure: (a) Helical trajectory comparison under 5 N load. (b) Euclidean distance between the reference EE position and the FK solution.

Stiffness Analysis at the End-Effector

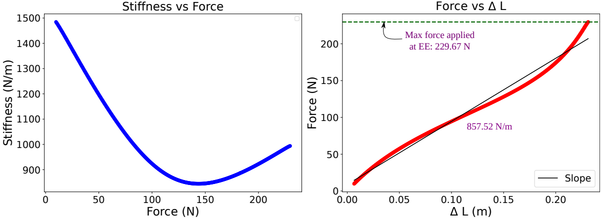

Figure: Stiffness analysis at the end-effector for increasing external compressive forces along the z-axis.

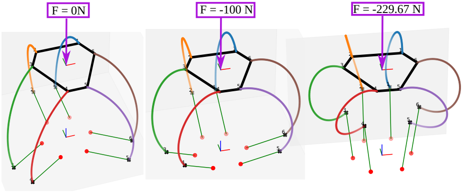

Figure: Deformed pose due to increasing external compressive force at a constant end-effector pose.

Rotation Capability at the End-Effector

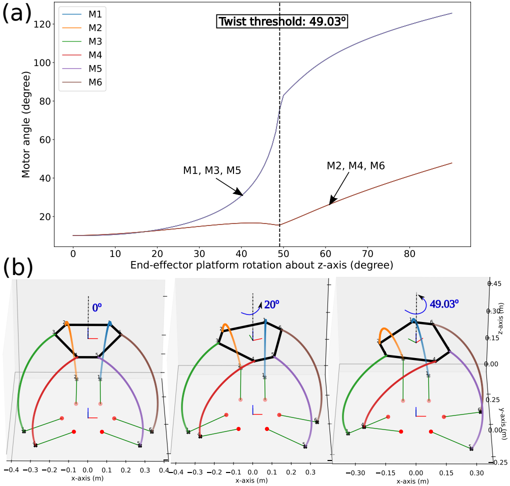

Figure: (a) Motor angle trajectories duuring rotation. (b) IK solution for a rotated EE platform about the z-axis.

Reachable Workspace Evaluation

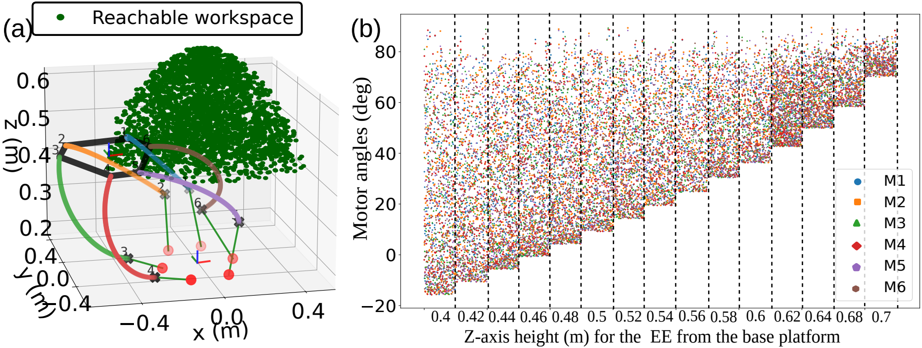

Figure: (a)Reachable workspace for the PKM (avg. computational time of 2.7s with ± 2.1) (b)Motor angle patterns for reachable workspace

Conclusion and Future work

Summary

- Cosserat Rod-based kinetostatic formulation: for both IK and FK.
- Maneuverability is analyzed through trajectory tracking in both 2D and 3D space under loading conditions.
- Stability analysis of the PCR under rotation about z-axis.
- Stiffness estimation with the compressive forces at the end-effector along z-axis
- Workspace analysis based on random 3D position of the end-effector.

Next step

- Improve the computational time especially for the initial value problem [5].
- Validation with the hardware with offline data.
- Performance comparison with FEM, data-driven methods .
- Influnece of no. of iterations on computational time and solution.

Acknowledgement

The work presented in this paper is supported by the PACOMA project (Grant No. ESA-TECMSM-SOW-022836) subcontracted to us by Airbus Defence & Space GmbH (Grant No. D.4283.01.02.01) with funds from the European Space Agency. The author also want to acknowledge John Till's GitHub tutorial on PCR and his guidance on the project.

References

1. C. E. Bryson and D. C. Rucker, "Toward parallel continuum manipulators," in 2014 IEEE International Conference on Robotics and Automation (ICRA), 2014, pp. 778-785.
2. M. T. Chikhaoui and B. Rosa, "Chapter 8 - modeling and control strategies for flexible devices in Endorobotics, L. Manfredi, Ed. Academic Press, 2022, pp. 187-213.
3. J. Till, C. E. Bryson, S. Chung, A. Orekhov, and D. C. Rucker, "Efficient computation of multiple coupled cosserat rod models for real-time simulation and control of paral- lel continuum manipulators," in 2015 IEEE International Conference on Robotics and Automation (ICRA), 2015, pp. 5067-5074.
4. C. B. Black, J. Till, and D. C. Rucker, "Parallel continuum robots: Modeling, analysis, and actuation-based force sensing," IEEE Transactions on Robotics, vol. 34, no. 1, pp. 29-47, 2018.

Thank You!